# REVISITING WEIGHT REGULARIZATION FOR LOW-RANK CONTINUAL LEARNING

**Anonymous authors**
Paper under double-blind review

## ABSTRACT

Continual Learning (CL) with large-scale pre-trained models (PTMs) has recently gained wide attention, shifting the focus from training from scratch to continually adapting PTMs. This has given rise to a promising paradigm: parameter-efficient continual learning (PECL), where task interference is typically mitigated by assigning a task-specific module during training, such as low-rank adapters. However, weight regularization techniques, such as Elastic Weight Consolidation (EWC)—a key strategy in CL—remain underexplored in this new paradigm. In this paper, we revisit weight regularization in low-rank CL as a new perspective for mitigating task interference in PECL. Unlike existing low-rank CL methods, we mitigate task interference by regularizing a shared low-rank update through EWC, thereby keeping the storage requirement constant regardless of the number of tasks. Moreover, we provide the first systematic investigation of EWC in low-rank CL, showing that it achieves a better stability–plasticity trade-off than other low-rank methods and enables competitive performance across a wide range of trade-off points. Building on these insights, we propose EWC-LoRA, which leverages a low-rank representation to estimate parameter importance over the full-dimensional space. This design offers a practical, computational- and memory-efficient solution for CL with PTMs, and provides insights that may inform the broader application of regularization techniques within PECL. Extensive experiments on various benchmarks demonstrate the effectiveness of EWC-LoRA. On average, EWC-LoRA improves over vanilla LoRA by 8.92% and achieves comparable or even superior performance to other state-of-the-art low-rank CL methods.

## 1 INTRODUCTION

Continual Learning (CL) (Parisi et al., 2019) has emerged as a rapidly growing research area, aiming to enable machine learning systems to acquire new knowledge without forgetting previously learned concepts. This ability plays a crucial role in addressing real-world problems (Shaheen et al., 2022; Wang et al., 2024a) where data distributions are constantly changing. Ideally, a CL model should maintain stable performance across all previously encountered tasks. A significant decline in performance on previous tasks after learning new ones is known as catastrophic forgetting (McCloskey & Cohen, 1989; Ratcliff, 1990), which typically arises from task interference.

With the rise of large-scale pre-trained models (PTMs) (Bommasani, 2021; Awais et al., 2025), the research focus in CL has shifted from training models from scratch to continually adapting these powerful models (Ostapenko et al., 2022; Yang et al., 2025). This trend is driven by the impressive transferability and robustness of PTMs, and a growing body of work has shown promising results in PTM-based continual adaptation. A particularly popular paradigm is parameter-efficient continual learning (PECL) (Qiao & Mahdavi, 2024), in which the PTM is typically kept frozen and augmented with lightweight modules such as prompts (Wang et al., 2022c; Smith et al., 2023), adapters (Ermis et al., 2022; Gao et al., 2024), or low-rank adaptations (LoRA) (Liang & Li, 2024; Wu et al., 2025). The predominant strategy in these works is to prevent task interference by assigning task-specific modules during training—either structurally isolated adapters or LoRA modules, or prompts that provide task-specific conditioning at the feature level.

On the other hand, weight regularization as a key continual learning strategy remains underexplored in the era of continual learning with PTMs. A canonical example is Elastic Weight Consolidation

(EWC) (Kirkpatrick et al., 2017), which has played a central role in combating catastrophic forgetting in small-scale models (Schwarz et al., 2018; Ehret et al., 2020). Although effective for smaller models, EWC is difficult to apply to PTMs, as estimating parameter importance via the Fisher Information Matrix (FIM) is computationally expensive, requiring storage of a frozen copy of the old model and a Fisher matrix of equal size, resulting in a memory overhead three times that of the original model. Several studies have attempted to apply EWC to the fine-tuning of large language models (Xiang et al., 2023; Šliogeris et al., 2025). However, they typically fine-tune the model with a precomputed Fisher matrix that is fixed throughout training, making them impractical for CL.

In this paper, we adopt EWC as a canonical example to study weight regularization in low-rank CL, systematically analyzing key considerations for applying EWC within low-rank adaptations and proposing a feasible weight-regularization-based solution for low-rank CL. *First, we revisit weight regularization in low-rank CL as a new perspective to mitigating catastrophic forgetting.* Existing low-rank CL methods assign each task an independent LoRA module, constraining updates to subspaces that reduce interference with prior tasks. While effective, the addition of LoRA modules incurs storage overhead that scales linearly with the number of tasks. In contrast, we mitigate task interference by regularizing a shared low-rank update through EWC, rather than structurally isolating task-specific parameters, thereby keeping the storage requirement constant regardless of the number of tasks. *Moreover, we provide the first systematic investigation of EWC in low-rank CL and propose a principled method to estimate the importance of parameters in the low-rank space.* The proposed method leverages the FIM to quantify each parameter's contribution more reliably while mitigating task interference. We empirically show that the regularization on low-rank matrices achieves a better stability–plasticity trade-off than other low-rank methods. Furthermore, the tunability of EWC enables competitive performance across a wide range of trade-off points.

Drawing on these insights, we propose **EWC-LoRA**, which updates the model via low-rank adaptation while leveraging the full-dimensional space FIM for weight regularization. EWC-LoRA does not explicitly fine-tune the full model or store model components for all previous tasks, thereby significantly reducing computational and memory overhead while enabling effective Fisher estimation, making it a resource-efficient solution for CL with PTMs. The main contributions of this work are as follows:

- We revisit weight regularization as a new perspective for mitigating catastrophic forgetting in low-rank CL. By exploiting the low-rank structure, we develop an efficient realization of EWC in PTMs. Specifically, by regularizing a shared LoRA module, EWC-LoRA maintains a constant memory footprint regardless of the number of tasks.
- We present the first systematic investigation of EWC in low-rank CL and propose estimating the FIM over the full-dimensional space to accurately capture parameter importance. As a result, EWC-LoRA achieves effective regularization and demonstrates a superior stability–plasticity trade-off compared to existing low-rank CL methods.
- Extensive experiments across multiple benchmarks demonstrate that EWC-LoRA is effective, improving over vanilla LoRA by an average of 8.92%, while achieving comparable or even superior performance to state-of-the-art low-rank CL methods, with better computational and storage efficiency.

## 2 Related Works

**Continual Learning (CL).** In contrast to standard supervised learning, which assumes that training data are independent and identically distributed (i.i.d.), CL focuses on training models on data streams that exhibit non-stationary and often continuous distribution shifts (Lesort et al., 2021). This departure from the i.i.d. assumption introduces the central challenge of catastrophic forgetting, where the model experiences significant performance degradation on previously learned tasks as new tasks are introduced (McCloskey & Cohen, 1989; Ratcliff, 1990). As summarized by Van de Ven & Tolias (2019), CL can be categorized into three main scenarios: task-incremental (Gao et al., 2023), domain-incremental (Wang et al., 2024b), and class-incremental learning (Hersche et al., 2022). Among these, class-incremental learning can be considered the most challenging. *In this work, we adhere to the class-incremental learning setting, where the model must learn to distinguish between all classes encountered across all tasks without explicit task boundaries* (Masana et al., 2022).

**Parameter-Efficient Continual Learning (PECL).** PECL (Qiao & Mahdavi, 2024) has recently emerged as a promising paradigm in CL. It builds upon the idea of parameter-efficient fine-tuning (Houlsby et al., 2019; Hu et al., 2022; Jia et al., 2022), where a pre-trained model is kept frozen and a small number of learnable parameters are introduced to adapt to new tasks. To prevent task interference, existing PECL methods can be categorized into two types: (1) prompt-based methods, which typically provide each task with task-specific prompts to condition PTMs at feature level (Wang et al., 2022c;b; Smith et al., 2023), and (2) adapter- or low-rank adaptation-based methods, which typically insert task-specific lightweight modules during training, thereby providing isolation at the structural level (Gao et al., 2024; Liang & Li, 2024; Wu et al., 2025). Existing PECL works thus primarily focus on introducing task-specific modules to mitigate task interference, which often leads to increased memory and computational costs as the number of tasks grows. In contrast, weight regularization techniques have received little attention, and it remains unclear how they can be effectively applied in PECL—a setting that presents unique structural and optimization challenges compared to full-model tuning. *Within the context of low-rank CL, we revisit weight regularization as a means to mitigate task interference, providing insights that may inform the broader application of regularization techniques within PECL—an area that remains underexplored in the current literature.*

**Elastic Weight Consolidation (EWC).** EWC (Kirkpatrick et al., 2017) mitigates catastrophic forgetting in CL by penalizing changes to parameters that are deemed important for previous tasks, as quantified by the Fisher Information Matrix (FIM). As a canonical example of weight regularization techniques, EWC has inspired a series of follow-up studies that aimed to address its limitations and broaden its applicability. For example, Huszár (2018) analyzed its behavior beyond two tasks, while van de Ven (2025) investigated strategies for estimating the FIM in the context of CL. In the era of PTMs, Xiang et al. (2023) apply EWC during fine-tuning of a large language model (LLM), using a precomputed FIM to protect the knowledge acquired by the original model. Similarly, Šliogeris et al. (2025) employ EWC in the context of LLMs, estimating the FIM on a comprehensive benchmark to preserve domain knowledge. However, both studies rely on a precomputed FIM, which is kept fixed throughout training, making them unsuitable for our setting. Thede et al. (2024) briefly note the continued value of regularization in the context of PTMs, but they do not examine its detailed effect and do not combine regularization with low-rank adaptation. Wei et al. (2025) do combine EWC with low-rank adaptation, but they separately regularize each low-rank module, causing inaccurate Fisher estimation and suboptimal performance. *Unlike prior work, we conduct a focused investigation of EWC in PTMs-based CL. By leveraging a low-rank structure, we propose a practical approach for adapting EWC to PTM-based CL and demonstrate its effectiveness.*

# 3 METHODOLOGY

In this section, we review the necessary preliminaries, then discuss the structural and optimization challenges of applying EWC to low-rank adaptation, and finally present an overview of EWC-LoRA, highlighting its learning procedure and differences from existing low-rank CL methods.

## 3.1 PRELIMINARIES

**Notations.** In this paper, bold lowercase letters represent vectors, while bold uppercase letters denote matrices. The superscript $\top$ indicates the transpose of a matrix, and $\mathbb{E}[\cdot]$ stands for the expectation operator. Optimal values of variables are indicated with a superscript $^*$.

**Problem Formulation.** We start with a pre-trained model parameterized by $\mathbf{W}_0$ and fine-tune it sequentially on a series of new tasks $\{\mathcal{T}_t\}_{t=1}^{T}$ with corresponding datasets $\{\mathcal{D}_t\}_{t=1}^{T}$. For each task $\mathcal{T}_t$, the model receives a batch of samples $\{x_k^t, y_k^t\}_{k=1}^{|\mathcal{D}_t|}$ drawn from $C$ classes, where $x_k^t$ and $y_k^t$ denote the input image and its corresponding label, respectively. After completing training on $\mathcal{T}_t$, the model is evaluated on all so-far encountered tasks $\mathcal{T}_{1:t}$. The objective is to learn parameters $\mathbf{W}$ that generalize well across all tasks so far, without storing any past data. With the model parameterized by $\mathbf{W}$, the training loss function at task $\mathcal{T}_t$ is usually defined as:

$$\mathcal{L}_t(\mathbf{W}) \;=\; -\frac{1}{|\mathcal{D}_t|}\sum_{k=1}^{|\mathcal{D}_t|}\sum_{c=1}^{C}\mathbb{1}_{[y_k^t=c]}\log p_{\mathbf{W}}(y=c \mid x_k^t) \tag{1}$$

**Elastic Weight Consolidation.** Following (Huszár, 2018), we maintain a single penalty term that approximates the combined effect of all previous tasks, preventing the double-counting inherent in the multi-penalty approach. When learning on task $\mathcal{T}_t$, we approximate the posterior $p(\mathbf{W}|\mathcal{D}_{1:t-1})$ using the Laplace approximation (MacKay, 1992), forming a Gaussian distribution $\mathcal{N}(\mathbf{W}; \mathbf{W}^*_{t-1}, (\mathbf{F}^{\text{cum}}_{t-1})^{-1})$, where $\mathbf{W}^*_{t-1}$ denotes the optimal parameters on task $\mathcal{T}_{1:t-1}$, and the accumulated Fisher matrix $\mathbf{F}^{\text{cum}}_{t-1}$ serves as the precision matrix, reflecting the importance of each parameter for retaining knowledge from all previous tasks. To improve computational efficiency, EWC assumes parameter independence and retains only the diagonal elements of the Fisher matrix. During training on $\mathcal{T}_t$, the loss function in Eq. 1 is augmented with a quadratic penalty term that constrains important parameters to remain close to their previously learned values:

$$\mathcal{L}'_t(\mathbf{W}) \;=\; \mathcal{L}_t(\mathbf{W}) \;+\; \frac{\lambda}{2}(\mathbf{W} - \mathbf{W}^*_{t-1})^\top \operatorname{diag}(\mathbf{F}^{\text{cum}}_{t-1})(\mathbf{W} - \mathbf{W}^*_{t-1}) \tag{2}$$

where $\lambda$ is a hyperparameter that controls the relative importance of the new task compared to the old one(s). $\operatorname{diag}(\mathbf{F}^{\text{cum}}_{t-1})$ denotes the diagonal matrix formed from the diagonal elements of the accumulated Fisher matrix. Hereafter, unless otherwise stated, $\mathbf{F}$ refers to the diagonal Fisher matrix, with the $\operatorname{diag}(\cdot)$ omitted for simplicity.

**Low-rank Adaptation (LoRA).** When fine-tuning a model, LoRA (Hu et al., 2022) restricts changes to the parameters to lie in a low-rank subspace. Suppose $\mathbf{W}, \mathbf{W}_0 \in \mathbb{R}^{d_O \times d_I}$ are the adapted and pre-trained weight matrix, respectively. LoRA expresses the weight update $\Delta\mathbf{W} = \mathbf{W} - \mathbf{W}_0$ as the product of two learnable matrices $\mathbf{A} \in \mathbb{R}^{d_O \times r}$ and $\mathbf{B} \in \mathbb{R}^{r \times d_I}$, with $r \ll \min(d_I, d_O)$. Thus, the adapted weight matrix can be represented as $\mathbf{W} = \mathbf{W}_0 + \Delta\mathbf{W} = \mathbf{W}_0 + \mathbf{AB}$. During fine-tuning, the pre-trained weights $\mathbf{W}_0$ are frozen and only the parameters of $\mathbf{A}$ and $\mathbf{B}$ are trainable.

### 3.2 EWC WITH LOW-RANK ADAPTATION

The core idea of EWC in Eq. 2 lies in the second term, which measures how far the current parameters deviate from the previously learned ones. Directly applying EWC entails fine-tuning all parameters, as well as preserving both a frozen copy of the old model and a Fisher matrix of the same size. However, in the case of large PTMs, this is often not feasible. To reduce the number of trainable parameters and improve efficiency, we represent the weight update as $\Delta\mathbf{W} = \mathbf{W} - \mathbf{W}^*_{t-1} = \mathbf{AB}$ via low-rank decomposition.

To regularize low-rank matrices, a straightforward way is to compute individual Fisher matrices for $\mathbf{A}$ and $\mathbf{B}$, and apply regularization to each accordingly (Wei et al., 2025). However, under low-rank parameterization, focusing solely on the individual low-rank matrices ignores the interaction between $\mathbf{A}$ and $\mathbf{B}$, which is problematic because each element of the update $\Delta\mathbf{W}$ depends on their joint product, i.e., $\Delta\mathbf{W}_{ij} = \sum_{k=1}^{r} \mathbf{A}_{ik}\mathbf{B}_{kj}$. In Appendix A.1.1, we mathematically prove that regularization performed separately in the low-rank space generally diverges from that performed in the full-dimensional space. Another way to regularize low-rank matrices is to precompute the Fisher matrix on the pre-trained model and then apply the regularization to the update $\Delta\mathbf{W} = \mathbf{AB}$ using this fixed Fisher matrix (Xiang et al., 2023). However, this estimation also includes directions associated with the frozen $\mathbf{W}_0$, which can introduce noise in measuring sensitivity to the loss. This issue is further illustrated in Appendix A.1.2.

To address the above limitations, we propose updating parameters in the low-rank space while regularizing over the full-dimensional subspace of $\mathbf{W}$ spanned by $\mathbf{A}$ and $\mathbf{B}$, as illustrated in Figure 1 (b). This ensures that the penalty captures the true sensitivity of the model output to low-rank updates, rather than merely the local gradient magnitudes. Consequently, we reformulate Eq. 2 as:

$$\mathcal{L}'_t(\mathbf{A}, \mathbf{B}) = \mathcal{L}_t(\mathbf{A}, \mathbf{B}) + \frac{\lambda}{2} \operatorname{vec}(\mathbf{AB})^\top \mathbf{F}^{\text{cum}}_{t-1} \operatorname{vec}(\mathbf{AB}) \tag{3}$$

where $\operatorname{vec}(\mathbf{AB})$ is flattened $\mathbf{AB}$. This formulation enables regularization in the full-dimensional subspace $\Delta\mathbf{W}$, without requiring explicit storage of $\operatorname{vec}(\mathbf{AB})$. After training on $\mathcal{T}_t$, we estimate $\mathbf{F}_t$ and incorporate it into the previously accumulated Fisher matrix to obtain the updated Fisher $\mathbf{F}^{\text{cum}}_t$.

To estimate the Fisher matrix $\mathbf{F}_t$ at the optimal parameters $\mathbf{W}^*_t$ for task $\mathcal{T}_t$, we follow the definition in (Martens, 2020). Specifically, the $i$-th diagonal element of $\mathbf{F}_t$ is defined as:

$$F_t^{i,i} = \mathbb{E}_{x \sim \mathcal{D}_t}\left[\mathbb{E}_{y \sim p_{\mathbf{W}^*_t}}\left[\left(\frac{\partial \log p_{\mathbf{W}}(y|x)}{\partial w_i}\bigg|_{\mathbf{W}=\mathbf{W}^*_t}\right)^2\right]\right] \tag{4}$$

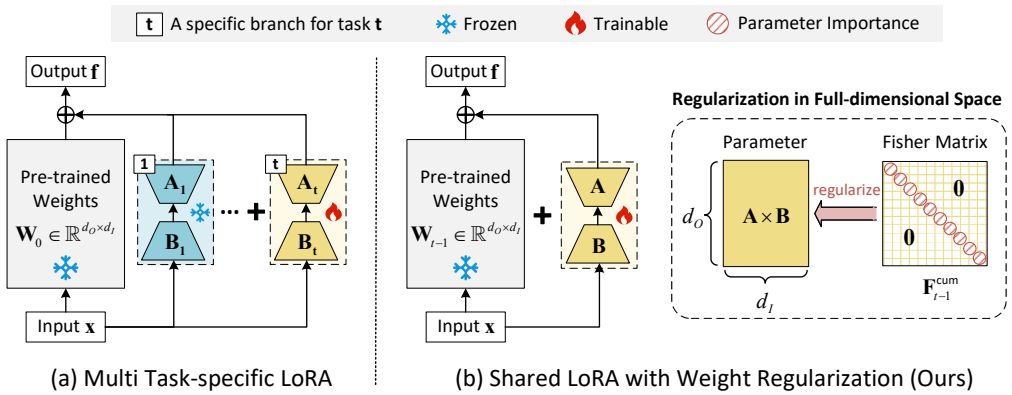


Figure 1: Overview of learning task $\mathcal{T}_t$ at a specific layer of the ViT model. **(a)** Prior low-rank CL methods structurally isolate task-specific LoRA parameters by adding a new LoRA branch for each task. **(b)** The proposed EWC-LoRA employs a shared LoRA module that is learned across all tasks and regularized according to parameter importance measured by a Fisher Information Matrix, which is updated after learning each task.

The outer expectation in Eq. 4 is computed over the current task data $\mathcal{D}_t$, while the inner expectation is approximated using the empirical Fisher for computational efficiency. In practice, this inner expectation can be estimated by taking the squared gradients of the log-likelihood with respect to $\mathbf{W}$, evaluated at $\mathbf{W}_t^*$. Since only the low-rank update $\Delta\mathbf{W}$ is trainable, the gradient with respect to $\mathbf{W}$ and $\Delta\mathbf{W}$ are identical. Consequently, the Fisher matrix is effectively computed in the $\Delta\mathbf{W}$-space. The equivalence between estimating the Fisher information in the $\mathbf{W}$-space and in the $\Delta\mathbf{W}$-space is established in Appendix A.1.3.

### 3.3 Overview of EWC-LoRA

Figure 1 illustrates the difference between EWC-LoRA and existing state-of-the-art low-rank CL methods, in the context of learning task $\mathcal{T}_t$ at a specific layer of the Vision Transformer (ViT). For task $\mathcal{T}_t$, we initialize the shared LoRA branch, and the forward computation is given by: $\mathbf{f} = \mathbf{W}_{t-1}\mathbf{x} + \mathbf{ABx}$. Specifically, $\mathbf{A}$ is zero-initialized, while $\mathbf{B}$ is drawn from a uniform distribution. During training on $\mathcal{T}_t$, only $\mathbf{A}$ and $\mathbf{B}$ are updated, while the base weights $\mathbf{W}_{t-1}$ keep frozen. After completing task $\mathcal{T}_t$, the learned parameters are integrated to the base weight as $\mathbf{W}_t = \mathbf{W}_{t-1} + \mathbf{AB}$. For any sample from a previous task, the forward computation becomes $\mathbf{f} = \mathbf{W}_t\mathbf{x}$. During training, the update of the low-rank matrices $\mathbf{A}$ and $\mathbf{B}$ are regularized using the accumulated Fisher matrix $\mathbf{F}_{t-1}^{\text{cum}}$ from step $t-1$. Accordingly, EWC-LoRA maintains only two states after learning step $t$: (1) the updated model parameters $\mathbf{W}_t$ obtained from the current task $\mathcal{T}_t$, and (2) the accumulated Fisher matrix $\mathbf{F}_t^{\text{cum}}$, a diagonal matrix that aggregates information from all previous tasks $\mathcal{T}_{1:t}$. The dataset $\mathcal{D}_t$ and the task-specific Fisher matrix $\mathbf{F}_t$ can then be discarded. For clarity, we outline the learning procedure of EWC-LoRA in Algorithm 1, provided in Appendix A.2.1.

## 4 Experiments

### 4.1 Benchmarks

**Datasets.** In line with existing continual learning methods (Liang & Li, 2024; Wu et al., 2025), we evaluate the performance of EWC-LoRA across four widely used continual learning benchmarks. They are CIFAR-100 (Krizhevsky et al., 2009), DomainNet (Peng et al., 2019; Wang et al., 2022a), ImageNet-R (Hendrycks et al., 2021a; Wang et al., 2022b), and ImageNet-A (Hendrycks et al., 2021b). CIFAR-100 consists of 100 natural image classes and is the most commonly used dataset in continual learning. DomainNet includes 345 classes across six diverse visual domains, making it a challenging multi-domain benchmark. ImageNet-R contains 200 ImageNet classes (Deng et al., 2009) rendered with various artistic styles, introducing significant distribution shifts. ImageNet-A consists of 200 natural adversarial examples that are frequently misclassified by standard ImageNet-

trained models. We follow the mostly used task splits for continual learning benchmarks: CIFAR-100 is divided into 10 tasks (10 classes per task); DomainNet into 5 tasks (69 classes per task); ImageNet-A into 10 tasks (20 classes each); ImageNet-R into 5, 10, and 20 tasks (with 40, 20, and 10 classes per task, respectively).

**Evaluation metrics.** We adopt accuracy as our evaluation metric, in line with standard practice (Lopez-Paz & Ranzato, 2017; Chaudhry et al., 2019). Let $A_{t,i}$ denote the classification accuracy on the $i$-th task after training on the $t$-th task. The average accuracy at learning step $t$ is defined as: $\overline{A}_t = \frac{1}{t}\sum_{i=1}^{t} A_{t,i}$. The overall average accuracy is then computed as the mean of all intermediate averages: Avg. $= \frac{1}{T}\sum_{t=1}^{T} \overline{A}_t$, where $T$ is the total number of tasks.

To further analyze a model's stability and plasticity and to enable intuitive comparisons across tasks, we propose measuring each metric on a normalized scale. Specifically, the stability score is defined as one minus the normalized forgetting:

$$\text{Stability} = 1 - \overline{F} = 1 - \frac{1}{T-1}\sum_{i=1}^{T-1} \frac{\max_{t<T} A_{t,i} - A_{T,i}}{\max_{t<T} A_{t,i}} \tag{5}$$

where normalized forgetting $\overline{F}$ represents the relative drop in a task's performance from its peak to the end of continual learning. For each task $i$, plasticity is defined as the ratio between the model's performance on the task after learning it and the corresponding reference performance. The overall plasticity is defined as:

$$\text{Plasticity} = \frac{1}{T}\sum_{i=1}^{T} \frac{A_{i,i}}{A_{i,i}^{\text{ref}}} \tag{6}$$

where $A_{i,i}^{\text{ref}}$ denotes the accuracy obtained by fine-tuning a model exclusively on task $i$. This normalization facilitates intuitive comparison across tasks and methods.

**Implementation details.** Following prior works (Wang et al., 2022c; Smith et al., 2023; Liang & Li, 2024), we adopt the ViT-B/16 backbone (Dosovitskiy et al., 2020) pretrained on ImageNet-21K in a supervised manner as the initialization for all models. To facilitate comparison, all methods are implemented within a unified framework. We align the experimental setup with that of InfLoRA (Liang & Li, 2024), fine-tuning the model with the Adam optimizer using hyperparameters $\beta_1 = 0.9$, $\beta_2 = 0.999$. For each comparison method, we report the best results using the hyperparameters provided by the authors whenever available. In cases where such configurations are not released, we apply a unified set of hyperparameters that has been validated to perform reliably across all methods, ensuring consistency in our experimental setup. To better contextualize performance, we report both an upper target (*Joint Train*) and a lower target (*Finetune*). The upper target jointly trains on all tasks, while the lower target sequentially trains on tasks without any forgetting mitigation. For all experiments, we perform five runs with different seeds and report the average and standard deviation of the results.

### 4.2 Main Results

**Comparison with Various CL Baselines.** We benchmark EWC-LoRA against state-of-the-art PTM-based continual learning methods, including the prompt-based methods L2P (Wang et al., 2022c), DualPrompt (Wang et al., 2022b), and CODA-Prompt (Smith et al., 2023), as well as the LoRA-based methods InfLoRA (Liang & Li, 2024) and SD-LoRA (Wu et al., 2025). We report results on 10 sequential tasks for CIFAR-100, ImageNet-R, and ImageNet-A, and on 5 tasks for DomainNet. The results are summarized in Table 1. We observe that EWC-LoRA achieves the highest final accuracy on three out of four datasets. On average, across all four datasets, EWC-LoRA outperforms vanilla LoRA by a substantial margin of +8.92%. EWC-LoRA even surpasses other LoRA-based methods that use task-specific low-rank modules, highlighting its effectiveness. Figure 2 illustrates the task-wise performance of LoRA-based methods. We observe that EWC-LoRA consistently outperforms other methods throughout the entire task sequence on most datasets, while also exhibiting lower standard deviations, indicating greater stability.

Table 1: Comparison results on CIFAR-100, DomainNet, ImageNet-R, and ImageNet-A (in %). **Bold** and underline indicate the highest and second-highest scores, respectively.

| Tasks | CIFAR-100 | | DomainNet | | ImageNet-R | | ImageNet-A | |
|---|---|---|---|---|---|---|---|---|
| Methods | $\overline{A}_{10}$ (↑) | Avg. (↑) | $\overline{A}_{5}$ (↑) | Avg. (↑) | $\overline{A}_{10}$ (↑) | Avg. (↑) | $\overline{A}_{10}$ (↑) | Avg. (↑) |
| Joint Train | $92.82_{(0.20)}$ | $95.41_{(0.05)}$ | $76.84_{(0.06)}$ | $81.25_{(0.05)}$ | $81.69_{(0.28)}$ | $86.25_{(0.09)}$ | $65.01_{(0.74)}$ | $74.10_{(0.44)}$ |
| Finetune | $79.09_{(1.53)}$ | $88.17_{(0.45)}$ | $65.57_{(0.20)}$ | $75.12_{(0.12)}$ | $60.42_{(1.64)}$ | $73.18_{(0.32)}$ | $32.85_{(1.53)}$ | $54.55_{(1.44)}$ |
| L2P | $83.18_{(1.20)}$ | $87.69_{(1.05)}$ | $70.26_{(0.25)}$ | $75.83_{(0.98)}$ | $71.26_{(0.44)}$ | $76.13_{(0.46)}$ | $42.94_{(1.27)}$ | $51.40_{(1.95)}$ |
| DualPrompt | $81.48_{(0.86)}$ | $86.41_{(0.66)}$ | $68.26_{(0.90)}$ | $73.84_{(0.45)}$ | $68.22_{(0.20)}$ | $73.81_{(0.39)}$ | $45.49_{(0.96)}$ | $54.68_{(1.24)}$ |
| CODA-Prompt | $86.31_{(0.12)}$ | $90.67_{(0.22)}$ | $70.58_{(0.53)}$ | $76.68_{(0.44)}$ | $74.05_{(0.41)}$ | $78.14_{(0.39)}$ | $45.36_{(0.78)}$ | $57.03_{(0.94)}$ |
| InfLoRA | $86.34_{(0.76)}$ | $\underline{91.33}_{(0.48)}$ | $71.01_{(0.05)}$ | $\underline{77.75}_{(0.03)}$ | $\mathbf{74.41}_{(0.63)}$ | $\mathbf{80.31}_{(0.60)}$ | $50.75_{(1.33)}$ | $64.36_{(1.01)}$ |
| SD-LoRA | $\underline{86.77}_{(0.30)}$ | $90.96_{(0.30)}$ | $\underline{71.27}_{(0.14)}$ | $77.70_{(0.07)}$ | $\underline{72.93}_{(2.76)}$ | $\underline{79.80}_{(0.15)}$ | $\underline{55.23}_{(0.94)}$ | $\underline{66.10}_{(0.54)}$ |
| Vanilla LoRA | $82.99_{(0.84)}$ | $89.74_{(0.58)}$ | $69.79_{(0.11)}$ | $77.44_{(0.08)}$ | $64.87_{(0.73)}$ | $75.57_{(0.23)}$ | $40.01_{(1.32)}$ | $58.28_{(0.85)}$ |
| EWC-LoRA | $\mathbf{87.91}_{(0.57)}$ | $\mathbf{92.27}_{(0.39)}$ | $\mathbf{73.46}_{(0.16)}$ | $\mathbf{79.58}_{(0.10)}$ | $72.86_{(0.79)}$ | $78.95_{(0.86)}$ | $\mathbf{59.89}_{(0.26)}$ | $\mathbf{68.33}_{(0.67)}$ |

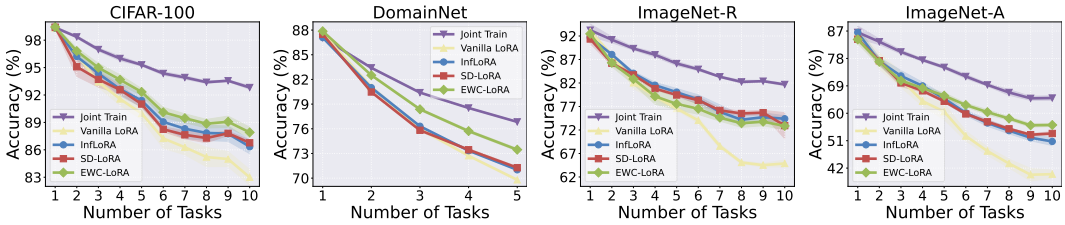


Figure 2: Task-wise performance comparison of different methods across various datasets.

**Analysis on Stability and Plasticity.** We evaluated both stability and plasticity for different low-rank CL methods across the four datasets. Stability reflects the ability of the model to retain previously learned knowledge, while plasticity measures its ability to adapt to new tasks. The results are reported in Table 2. As expected, Vanilla LoRA typically exhibits the highest plasticity but the lowest stability, since it employs no strategy to mitigate catastrophic forgetting. We observe that InfLoRA emphasizes stability, while SD-LoRA favors plasticity. On CIFAR-100, EWC-LoRA matches InfLoRA in stability while achieving higher plasticity; on ImageNet-A, it matches SD-LoRA in plasticity while providing greater stability. On DomainNet and ImageNet-R, while other methods struggle to balance stability and plasticity, EWC-LoRA can achieve this trade-off effectively by tuning the regularization strength $\lambda$.

Table 2: Stability (↑) and plasticity (↑) scores of different low-rank CL methods, reflecting how well each model retains previous knowledge and adapts to new tasks. We report the normalized form of the two metrics, which is independent of the absolute performance on the dataset.

| Tasks | CIFAR-100 | | DomainNet | | ImageNet-R | | ImageNet-A | |
|---|---|---|---|---|---|---|---|---|
| Methods | Stability | Plasticity | Stability | Plasticity | Stability | Plasticity | Stability | Plasticity |
| Vanilla LoRA | $87.56_{(0.09)}$ | $98.86_{(0.09)}$ | $81.29_{(0.34)}$ | $97.94_{(0.16)}$ | $78.63_{(1.38)}$ | $99.57_{(0.35)}$ | $85.56_{(1.82)}$ | $97.56_{(0.77)}$ |
| InfLoRA | $94.84_{(0.52)}$ | $95.80_{(1.00)}$ | $83.80_{(0.37)}$ | $97.34_{(0.29)}$ | $92.69_{(0.77)}$ | $97.33_{(0.46)}$ | $88.63_{(3.39)}$ | $72.69_{(3.13)}$ |
| SD-LoRA | $91.85_{(0.60)}$ | $98.24_{(0.25)}$ | $82.45_{(0.19)}$ | $98.69_{(0.15)}$ | $91.78_{(0.90)}$ | $95.61_{(0.32)}$ | $88.61_{(1.05)}$ | $92.13_{(2.77)}$ |
| EWC-LoRA | $94.45_{(0.59)}$ | $97.99_{(0.50)}$ | $91.51_{(0.36)}$ | $93.83_{(0.23)}$ | $95.62_{(0.42)}$ | $93.23_{(0.34)}$ | $89.52_{(1.14)}$ | $92.78_{(1.91)}$ |

Specifically, for the results in Table 1 and 2, a unified regularization strength is used across datasets. With $\lambda = 10^7$, EWC-LoRA consistently achieves a favorable balance between stability and plasticity, without requiring dataset-specific tuning. To explore the trade-off between the two metrics, we show stability–plasticity curves for different values of the regularization strength, as illustrated in Figure 3a. Unlike other methods that typically exhibit fixed performance, EWC-LoRA provides a clear and controllable trade-off: smaller $\lambda$ promotes plasticity at the cost of stability, while larger values enhance stability but reduce plasticity. This tunability enables EWC-LoRA to achieve competitive or superior performance across a wide range of trade-off points, demonstrating its robustness and adaptability. We also note that even when different methods achieve similar average accuracy, they can differ substantially in terms of stability and plasticity. This suggests that CL model evaluation should place greater emphasis on explicitly reporting stability and plasticity metrics.

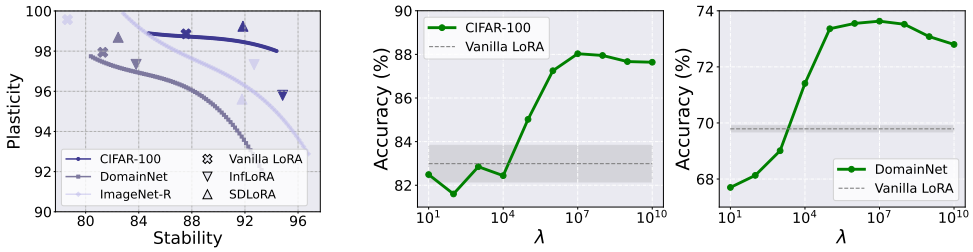


(a) Stability–Plasticity curves. (b) Performance across a range of regularization strengths $\lambda$.

Figure 3: (a) Stability–Plasticity curves illustrating the trade-off between retaining previous knowledge and learning new tasks. (b) Performance across a range of regularization strengths $\lambda$ on CIFAR-100 and DomainNet, showing the effect of $\lambda$ on accuracy.

**Memory footprint and training time.** The additional memory and computational cost of EWC-LoRA compared to Vanilla LoRA comes only from the FIM. After each learning step, the LoRA parameters are merged into the backbone, so the total parameter size matches that of the pre-trained model. As a result, only one shared LoRA is required for new tasks, and the memory footprint remains constant regardless of the number of tasks. In contrast, other low-rank CL methods require either maintaining separate LoRA parameters for each task or performing more complex computations, leading to a linear increase in memory usage and training time, or to higher computational cost as the number of tasks grows. EWC-LoRA incurs modest memory overhead during training while improving computational efficiency, achieving comparable or even superior performance.

Table 3: Comparison of different methods in terms of memory cost and training time. Memory usage is measured on the Quadro RTX 6000 GPU with a batch size of 128. Training time is reported as the average time required to train a single task.

| Methods | Memory | **CIFAR-100** | **DomainNet** | **ImageNet-R** | **ImageNet-A** |
|---|---|---|---|---|---|
| Vanilla LoRA | $\sim$ 18 GB | 10m22s $\pm$ 7s | 32m8s $\pm$ 44s | 13m32s $\pm$ 105s | 0m55s $\pm$ 21s |
| InfLoRA | $\sim$ 20 GB | 11m9s $\pm$ 4s | 42m25s $\pm$ 68s | 14m33s $\pm$ 107s | 1m16s $\pm$ 22s |
| SD-LoRA | $\sim$ 37 GB | 12m16s $\pm$ 86s | 34m18s $\pm$ 160s | 22m53s $\pm$ 232s | 1m56s $\pm$ 36s |
| EWC-LoRA | $\sim$ 24 GB | 10m31s $\pm$ 3s | 33m10s $\pm$ 50s | 13m42s $\pm$ 104s | 0m55s $\pm$ 21s |

The memory cost and training time are reported in Table 3. Memory usage is measured on two Quadro RTX 6000 GPUs with a batch size of 128. Training time is recorded as the average duration to train a single task, presented along with the standard deviation. Notably, the training time of EWC-LoRA is nearly identical to that of Vanilla LoRA, demonstrating that the additional computations introduced by Fisher estimation in the low-rank space incur only minimal overhead.

### 4.3 Ablation Study

**Results Across Varied Task Lengths.** We further examine the performance of different low-rank CL methods under varying task lengths. As a complementary study to Table 1, we split CIFAR-100 and ImageNet-R into 5-task and 20-task sequences, respectively. As reported in Table 4, the improvement is most evident on CIFAR-100, where EWC-LoRA achieves the highest overall accuracy among all methods. In contrast, the gains on ImageNet-R are more moderate, which may be attributed to the domain shift in ImageNet-R, potentially limiting the effectiveness of regularization-based approaches for continual adaptation. Additional results are provided in the Appendix A.3.

**Ablation on Regularization Strength $\lambda$.** We evaluate performance under varying values of the regularization strength $\lambda$, ranging from 10 to $10^{10}$. The results are presented in Figures 3b. We use empirical Fisher in all experiments. From the figures, we observe that setting $\lambda$ to $10^7$ allows EWC-LoRA to consistently achieve favorable performance in terms of accuracy, stability, and plasticity. This suggests that an appropriate balance between stability and plasticity can be effectively maintained without fine-grained tuning. This finding facilitates the use of a unified regularization strength across datasets, eliminating the need for dataset-specific tuning.

Table 4: Final accuracy on CIFAR-100 and ImageNet-R for task lengths of 5 and 20 tasks.

| Tasks | CIFAR-100 | | ImageNet-R | |
|---|---|---|---|---|
| Methods | $\overline{A}_5$ | $\overline{A}_{20}$ | $\overline{A}_5$ | $\overline{A}_{20}$ |
| Vanilla LoRA | 87.15 | 74.78 | 70.15 | 56.17 |
| InfLoRA | <u>89.45</u> | 81.77 | **77.37** | 69.63 |
| SD-LoRA | 89.15 | <u>83.57</u> | 74.90 | **72.26** |
| EWC-LoRA | **89.98** | **85.46** | <u>76.36</u> | <u>70.18</u> |

Table 5: Best performance with Exact Fisher (500 random samples) and Empirical Fisher.

| **Estimation** | **Exact (n=500)** | **Empirical** |
|---|---|---|
| $\overline{A}_{10}$ | 88.28 | 87.91 |
| Avg. | 92.76 | 92.27 |
| Best $\lambda$ | $\lambda = 10^5$ | $\lambda = 10^7$ |
| Training Time | $\sim$ 14m | $\sim$ 11m |
| Memory Cost | $\sim$ 20 GB | $\sim$ 24GB |

**Estimation of Fisher Information Matrix.** In the context of low-rank adaptation, we examine the trade-off between performance and the computational cost of estimating the Fisher Information Matrix, as discussed by van de Ven (2025). In general, the Exact Fisher outperforms the Empirical Fisher, requiring a smaller regularization strength. From a computational perspective, computing the Exact Fisher on a small batch of data yields superior results compared to the Empirical Fisher while significantly reducing computational overhead. We use 500 randomly selected samples to estimate the Exact Fisher, and the comparison results are shown in Table 5. We report both the training time for a single task and the corresponding memory usage. Additional results comparing different strategies for estimating the Fisher matrix are provided in Appendix A.3.

**Different Fisher Estimation Strategies.** We compare three different Fisher estimation strategies, based on the discussion in Section 3.2. "Precomputed $\mathbf{F_W}$" refers to using a precomputed FIM in full parameter space $\mathbf{W}$ to preserve prior knowledge. Instead of estimating over a large-scale dataset, we consider a dataset-based Fisher, computed using the entire dataset that will be learned sequentially. "Separate $\mathbf{F_A}, \mathbf{F_B}$" denotes estimating the Fisher separately for the low-rank matrices and regularizing them accordingly, while "$\mathbf{F}_{\Delta\mathbf{W}}$" denotes estimating the Fisher in the full-dimensional space as $\mathbf{W}$. The results are shown in Table 6. We observe that the precomputed Fisher results in the lowest plasticity, which may be caused by undesirable sensitivity arising from the frozen weights. Moreover, applying separate regularization in the low-rank space also improves performance but has noticeable drawbacks in terms of plasticity. This may be due to the joint contribution of the low-rank factors, which imposes stronger constraints on the parameters.

Table 6: Comparison of different Fisher estimation strategies on CIFAR-100. "**+ Mem.**" indicates the additional memory required for Fisher estimation and regularization during training.

| **Strategy** | $\overline{A}_{10}$ | Avg. | Stability | Plasticity | **+ Mem.** |
|---|---|---|---|---|---|
| w/o $\mathbf{F}$ | $82.99_{(0.84)}$ | $89.74_{(0.58)}$ | $87.56_{(0.09)}$ | $\mathbf{98.86}_{(0.09)}$ | 0 GB |
| Precomputed $\mathbf{F_W}$ | $83.87_{(0.21)}$ | $89.36_{(0.49)}$ | $93.15_{(0.45)}$ | $94.74_{(0.56)}$ | 1 GB |
| Separate $\mathbf{F_A}, \mathbf{F_B}$ | $86.41_{(0.69)}$ | $91.33_{(0.50)}$ | $94.23_{(0.46)}$ | $96.47_{(0.21)}$ | 4 GB |
| $\mathbf{F}_{\Delta\mathbf{W}}$ (Ours) | $\mathbf{87.91}_{(0.57)}$ | $\mathbf{92.27}_{(0.39)}$ | $\mathbf{94.45}_{(0.59)}$ | $97.99_{(0.50)}$ | 6 GB |

## 5 Conclusion and Discussion

In this work, we revisit weight regularization in low-rank continual learning (CL) as a means to mitigate catastrophic forgetting. Using Elastic Weight Consolidation (EWC) as a canonical example, we discuss the main considerations about applying regularization in the low-rank space and propose EWC-LoRA, a computational- and memory-efficient solution for low-rank CL with large pre-trained models. This work aims to offer insights that may guide the broader application of regularization techniques in parameter-efficient continual learning.

A key limitation of regularization-based low-rank CL methods is their sensitivity to dataset complexity. When combined with regularization techniques, it is important to carefully allocate the low-rank learnable space for each task. This sensitivity also helps explain why, on ImageNet-R, EWC-LoRA shows lower plasticity than methods based on task-specific modules. Consequently, a promising direction for future work is to investigate the performance of regularization techniques in domain-incremental settings and on more complex continual learning tasks.

## 6 REPRODUCIBILITY STATEMENT

The theoretical analysis and complete proofs of the main results are provided in Appendix A.1. The implementation details of our method, including model architecture, training procedures, and hyperparameters, are described in Section 3 of the main paper and Appendix A.2. All datasets used in our experiments are publicly available. The source code for reproducing results is available in the supplementary materials.

## REFERENCES

Muhammad Awais, Muzammal Naseer, Salman Khan, Rao Muhammad Anwer, Hisham Cholakkal, Mubarak Shah, Ming-Hsuan Yang, and Fahad Shahbaz Khan. Foundation models defining a new era in vision: a survey and outlook. IEEE Transactions on Pattern Analysis and Machine Intelligence, 2025.

Rishi Bommasani. On the opportunities and risks of foundation models. arXiv preprint arXiv:2108.07258, 2021.

Arslan Chaudhry, Marcus Rohrbach, Mohamed Elhoseiny, Thalaiyasingam Ajanthan, Puneet K Dokania, Philip HS Torr, and Marc'Aurelio Ranzato. On tiny episodic memories in continual learning. arXiv preprint arXiv:1902.10486, 2019.

Jia Deng, Wei Dong, Richard Socher, Li-Jia Li, Kai Li, and Li Fei-Fei. Imagenet: A large-scale hierarchical image database. In 2009 IEEE conference on computer vision and pattern recognition, pp. 248–255. Ieee, 2009.

Alexey Dosovitskiy, Lucas Beyer, Alexander Kolesnikov, Dirk Weissenborn, Xiaohua Zhai, Thomas Unterthiner, Mostafa Dehghani, Matthias Minderer, Georg Heigold, Sylvain Gelly, et al. An image is worth 16x16 words: Transformers for image recognition at scale. arXiv preprint arXiv:2010.11929, 2020.

Benjamin Ehret, Christian Henning, Maria R Cervera, Alexander Meulemans, Johannes Von Oswald, and Benjamin F Grewe. Continual learning in recurrent neural networks. arXiv preprint arXiv:2006.12109, 2020.

Beyza Ermis, Giovanni Zappella, Martin Wistuba, Aditya Rawal, and Cédric Archambeau. Continual learning with transformers for image classification. In Proceedings of the IEEE/CVF Conference on Computer Vision and Pattern Recognition, pp. 3774–3781, 2022.

Qiang Gao, Xiaojun Shan, Yuchen Zhang, and Fan Zhou. Enhancing knowledge transfer for task incremental learning with data-free subnetwork. Advances in Neural Information Processing Systems, 36:68471–68484, 2023.

Xinyuan Gao, Songlin Dong, Yuhang He, Qiang Wang, and Yihong Gong. Beyond prompt learning: Continual adapter for efficient rehearsal-free continual learning. In European Conference on Computer Vision, pp. 89–106. Springer, 2024.

Dan Hendrycks, Steven Basart, Norman Mu, Saurav Kadavath, Frank Wang, Evan Dorundo, Rahul Desai, Tyler Zhu, Samyak Parajuli, Mike Guo, et al. The many faces of robustness: A critical analysis of out-of-distribution generalization. In Proceedings of the IEEE/CVF international conference on computer vision, pp. 8340–8349, 2021a.

Dan Hendrycks, Kevin Zhao, Steven Basart, Jacob Steinhardt, and Dawn Song. Natural adversarial examples. CVPR, 2021b.

Michael Hersche, Geethan Karunaratne, Giovanni Cherubini, Luca Benini, Abu Sebastian, and Abbas Rahimi. Constrained few-shot class-incremental learning. In Proceedings of the IEEE/CVF conference on computer vision and pattern recognition, pp. 9057–9067, 2022.

Neil Houlsby, Andrei Giurgiu, Stanislaw Jastrzebski, Bruna Morrone, Quentin De Laroussilhe, Andrea Gesmundo, Mona Attariyan, and Sylvain Gelly. Parameter-efficient transfer learning for nlp. In International conference on machine learning, pp. 2790–2799. PMLR, 2019.

Edward J Hu, Yelong Shen, Phillip Wallis, Zeyuan Allen-Zhu, Yuanzhi Li, Shean Wang, Lu Wang, Weizhu Chen, et al. Lora: Low-rank adaptation of large language models. ICLR, 1(2):3, 2022.

Ferenc Huszár. Note on the quadratic penalties in elastic weight consolidation. Proceedings of the National Academy of Sciences, 115(11):E2496–E2497, 2018.

Menglin Jia, Luming Tang, Bor-Chun Chen, Claire Cardie, Serge Belongie, Bharath Hariharan, and Ser-Nam Lim. Visual prompt tuning. In European conference on computer vision, pp. 709–727. Springer, 2022.

James Kirkpatrick, Razvan Pascanu, Neil Rabinowitz, Joel Veness, Guillaume Desjardins, Andrei A Rusu, Kieran Milan, John Quan, Tiago Ramalho, Agnieszka Grabska-Barwinska, et al. Overcoming catastrophic forgetting in neural networks. Proceedings of the national academy of sciences, 114(13):3521–3526, 2017.

Alex Krizhevsky, Geoffrey Hinton, et al. Learning multiple layers of features from tiny images. 2009.

Timothée Lesort, Massimo Caccia, and Irina Rish. Understanding continual learning settings with data distribution drift analysis. arXiv preprint arXiv:2104.01678, 2021.

Yan-Shuo Liang and Wu-Jun Li. Inflora: Interference-free low-rank adaptation for continual learning. In Proceedings of the IEEE/CVF Conference on Computer Vision and Pattern Recognition, pp. 23638–23647, 2024.

David Lopez-Paz and Marc'Aurelio Ranzato. Gradient episodic memory for continual learning. Advances in neural information processing systems, 30, 2017.

David JC MacKay. A practical bayesian framework for backpropagation networks. Neural computation, 4(3):448–472, 1992.

James Martens. New insights and perspectives on the natural gradient method. Journal of Machine Learning Research, 21(146):1–76, 2020.

Marc Masana, Xialei Liu, Bartłomiej Twardowski, Mikel Menta, Andrew D Bagdanov, and Joost Van De Weijer. Class-incremental learning: survey and performance evaluation on image classification. IEEE Transactions on Pattern Analysis and Machine Intelligence, 45(5):5513–5533, 2022.

Michael McCloskey and Neal J Cohen. Catastrophic interference in connectionist networks: The sequential learning problem. In Psychology of learning and motivation, volume 24, pp. 109–165. Elsevier, 1989.

Oleksiy Ostapenko, Timothee Lesort, Pau Rodriguez, Md Rifat Arefin, Arthur Douillard, Irina Rish, and Laurent Charlin. Continual learning with foundation models: An empirical study of latent replay. In Conference on lifelong learning agents, pp. 60–91. PMLR, 2022.

German I Parisi, Ronald Kemker, Jose L Part, Christopher Kanan, and Stefan Wermter. Continual lifelong learning with neural networks: A review. Neural networks, 113:54–71, 2019.

Xingchao Peng, Qinxun Bai, Xide Xia, Zijun Huang, Kate Saenko, and Bo Wang. Moment matching for multi-source domain adaptation. In Proceedings of the IEEE/CVF international conference on computer vision, pp. 1406–1415, 2019.

Fuli Qiao and Mehrdad Mahdavi. Learn more, but bother less: parameter efficient continual learning. Advances in Neural Information Processing Systems, 37:97476–97498, 2024.

Roger Ratcliff. Connectionist models of recognition memory: constraints imposed by learning and forgetting functions. Psychological review, 97(2):285, 1990.

Jonathan Schwarz, Wojciech Czarnecki, Jelena Luketina, Agnieszka Grabska-Barwinska, Yee Whye Teh, Razvan Pascanu, and Raia Hadsell. Progress & compress: A scalable framework for continual learning. In International conference on machine learning, pp. 4528–4537. PMLR, 2018.

Khadija Shaheen, Muhammad Abdullah Hanif, Osman Hasan, and Muhammad Shafique. Continual learning for real-world autonomous systems: Algorithms, challenges and frameworks. Journal of Intelligent & Robotic Systems, 105(1):9, 2022.

Vytenis Šliogeris, Povilas Daniušis, and Artūras Nakvosas. Full-parameter continual pretraining of gemma2: Insights into fluency and domain knowledge. arXiv preprint arXiv:2505.05946, 2025.

James Seale Smith, Leonid Karlinsky, Vyshnavi Gutta, Paola Cascante-Bonilla, Donghyun Kim, Assaf Arbelle, Rameswar Panda, Rogerio Feris, and Zsolt Kira. Coda-prompt: Continual decomposed attention-based prompting for rehearsal-free continual learning. In Proceedings of the IEEE/CVF conference on computer vision and pattern recognition, pp. 11909–11919, 2023.

Lukas Thede, Karsten Roth, Olivier J Hénaff, Matthias Bethge, and Zeynep Akata. Reflecting on the state of rehearsal-free continual learning with pretrained models. arXiv preprint arXiv:2406.09384, 2024.

Gido M van de Ven. On the computation of the fisher information in continual learning. arXiv preprint arXiv:2502.11756, 2025.

Gido M Van de Ven and Andreas S Tolias. Three scenarios for continual learning. arXiv preprint arXiv:1904.07734, 2019.

Liyuan Wang, Xingxing Zhang, Hang Su, and Jun Zhu. A comprehensive survey of continual learning: Theory, method and application. IEEE transactions on pattern analysis and machine intelligence, 46(8):5362–5383, 2024a.

Qiang Wang, Yuhang He, Songlin Dong, Xinyuan Gao, Shaokun Wang, and Yihong Gong. Non-exemplar domain incremental learning via cross-domain concept integration. In European Conference on Computer Vision, pp. 144–162. Springer, 2024b.

Yabin Wang, Zhiwu Huang, and Xiaopeng Hong. S-prompts learning with pre-trained transformers: An occam's razor for domain incremental learning. Advances in Neural Information Processing Systems, 35:5682–5695, 2022a.

Zifeng Wang, Zizhao Zhang, Sayna Ebrahimi, Ruoxi Sun, Han Zhang, Chen-Yu Lee, Xiaoqi Ren, Guolong Su, Vincent Perot, Jennifer Dy, et al. Dualprompt: Complementary prompting for rehearsal-free continual learning. In European conference on computer vision, pp. 631–648. Springer, 2022b.

Zifeng Wang, Zizhao Zhang, Chen-Yu Lee, Han Zhang, Ruoxi Sun, Xiaoqi Ren, Guolong Su, Vincent Perot, Jennifer Dy, and Tomas Pfister. Learning to prompt for continual learning. In Proceedings of the IEEE/CVF conference on computer vision and pattern recognition, pp. 139–149, 2022c.

Xiwen Wei, Guihong Li, and Radu Marculescu. Online-lora: Task-free online continual learning via low rank adaptation. In 2025 IEEE/CVF Winter Conference on Applications of Computer Vision (WACV), pp. 6634–6645. IEEE, 2025.

Yichen Wu, Hongming Piao, Long-Kai Huang, Renzhen Wang, Wanhua Li, Hanspeter Pfister, Deyu Meng, Kede Ma, and Ying Wei. Sd-lora: Scalable decoupled low-rank adaptation for class incremental learning. arXiv preprint arXiv:2501.13198, 2025.

Jiannan Xiang, Tianhua Tao, Yi Gu, Tianmin Shu, Zirui Wang, Zichao Yang, and Zhiting Hu. Language models meet world models: Embodied experiences enhance language models. Advances in neural information processing systems, 36:75392–75412, 2023.

Yutao Yang, Jie Zhou, Xuanwen Ding, Tianyu Huai, Shunyu Liu, Qin Chen, Yuan Xie, and Liang He. Recent advances of foundation language models-based continual learning: A survey. ACM Computing Surveys, 57(5):1–38, 2025.

# A Appendix

## A.1 Theoretical Analysis

**Setup.** In low-rank adaptation, the adapted weight matrix $\mathbf{W} \in \mathbb{R}^{d_O \times d_I}$ is reparameterized as $\mathbf{W} = \mathbf{W}_0 + \Delta\mathbf{W} = \mathbf{W}_0 + \mathbf{AB}$, where $\mathbf{W}_0$ denotes the pre-trained weight, which remains frozen during fine-tuning. The trainable parameters are the low-rank matrices $\mathbf{A} \in \mathbb{R}^{d_O \times r}$ and $\mathbf{B} \in \mathbb{R}^{r \times d_I}$, such that $\Delta\mathbf{W} = \mathbf{AB}$ is the only trainable update to the model. Note that the learned LoRA modules on the previous task are merged back into the base weights before starting the new task. The optimal weight matrix is indicated as $\mathbf{W}^*$.

### A.1.1 Regularization under Different Parameterizations

**Proposition 1.** *Let $\Delta\mathbf{W} \in \mathbb{R}^{d_O \times d_I}$ be a model parameter matrix factorized as $\Delta\mathbf{W} = \mathbf{AB}$, with $\mathbf{A} \in \mathbb{R}^{d_O \times r}$, $\mathbf{B} \in \mathbb{R}^{r \times d_O}$. Define the EWC regularization term in the full-space as $\mathcal{R}_{\mathbf{W}}$, and in the low-rank parameter space as $\mathcal{R}_{\mathbf{A},\mathbf{B}}$. Under general conditions, $\mathcal{R}_{\Delta\mathbf{W}} \not\equiv \mathcal{R}_{\mathbf{A},\mathbf{B}}$.*

***Proof.*** Let $\mathrm{vec}(\cdot)$ denote the vectorization operator, and $\otimes$ the Kronecker product. The following identity holds:

$$\mathrm{vec}(\mathbf{AB}) = (\mathbf{B}^\top \otimes \mathbf{I}_{d_O})\,\mathrm{vec}(\mathbf{A}) = (\mathbf{I}_{d_I} \otimes \mathbf{A})\,\mathrm{vec}(\mathbf{B})$$

For simplicity, we define $\mathbf{a} = \mathrm{vec}(\mathbf{A}) \in \mathbb{R}^{d_O r}$, $\mathbf{b} = \mathrm{vec}(\mathbf{B}) \in \mathbb{R}^{r d_I}$. Define the Jacobians:

$$J_A(\mathbf{B}) := \mathbf{B}^\top \otimes \mathbf{I}_{d_O} \in \mathbb{R}^{d_O d_I \times d_O r}, \quad J_B(\mathbf{A}) := \mathbf{I}_{d_I} \otimes \mathbf{A} \in \mathbb{R}^{d_O d_I \times r d_I}$$

By the standard vectorization identity:

$$\mathrm{vec}(\Delta\mathbf{W}) = J_A(\mathbf{B})\mathbf{a} = J_B(\mathbf{A})\mathbf{b}$$

The Fisher Information Matrix estimated in the full-dimensional space is defined as:

$$\mathbf{F}_{\mathbf{W}} = \mathbb{E}_{x\sim\mathcal{D}}\left[\mathrm{vec}(\nabla_{\mathbf{W}}\mathcal{L})\,\mathrm{vec}(\nabla_{\mathbf{W}}\mathcal{L})^\top\right]$$

Although the full-space regularization $\mathcal{R}_{\mathbf{W}}$ can be expressed equivalently using either the $\mathbf{A}$ or $\mathbf{B}$ Jacobian, the update directions for $\mathbf{A}$ and $\mathbf{B}$ remain coupled. Thus, we consider a first-order approximation of $\mathrm{vec}(\Delta\mathbf{W})$ as a function of both $\mathbf{a}$ and $\mathbf{b}$:

$$\mathrm{vec}(\Delta\mathbf{W}) \approx J_A(\mathbf{B})\Delta\mathbf{a} + J_B(\mathbf{A})\Delta\mathbf{b}$$

The EWC regularization term in the full-space is defined as:

$$\begin{aligned}
\mathcal{R}_{\mathbf{W}} &= \frac{1}{2}(\mathrm{vec}(\mathbf{W}) - \mathrm{vec}(\mathbf{W}^*))^\top \mathbf{F}_{\mathbf{W}}(\mathrm{vec}(\mathbf{W}) - \mathrm{vec}(\mathbf{W}^*)) \\
&= \frac{1}{2}\,\mathrm{vec}(\Delta\mathbf{W})^\top \mathbf{F}_{\mathbf{W}}\,\mathrm{vec}(\Delta\mathbf{W}) \\
&= \frac{1}{2}\Delta\mathbf{a}^\top J_A(\mathbf{B})^\top \mathbf{F}_{\mathbf{W}} J_A(\mathbf{B})\Delta\mathbf{a} + \frac{1}{2}\Delta\mathbf{b}^\top J_B(\mathbf{A})^\top \mathbf{F}_{\mathbf{W}} J_B(\mathbf{A})\Delta\mathbf{b} \\
&\quad + \Delta\mathbf{a}^\top J_A(\mathbf{B})^\top \mathbf{F}_{\mathbf{W}} J_B(\mathbf{A})\Delta\mathbf{b}
\end{aligned}$$

If Fisher regularization is applied separately to $\mathbf{A}$ and $\mathbf{B}$, we have two Fisher matrices:

$$\begin{aligned}
\mathbf{F}_{\mathbf{A}} &= \mathbb{E}_{x\sim\mathcal{D}}\left[\mathrm{vec}(\nabla_{\mathbf{A}}\mathcal{L})\,\mathrm{vec}(\nabla_{\mathbf{A}}\mathcal{L})^\top\right] \\
\mathbf{F}_{\mathbf{B}} &= \mathbb{E}_{x\sim\mathcal{D}}\left[\mathrm{vec}(\nabla_{\mathbf{B}}\mathcal{L})\,\mathrm{vec}(\nabla_{\mathbf{B}}\mathcal{L})^\top\right]
\end{aligned}$$

By the chain rule, the gradients in low-rank factor space are related to the full-space gradient by:

$$\begin{aligned}
\nabla_{\mathbf{A}}\mathcal{L} &= \frac{\partial\mathcal{L}}{\partial\mathbf{W}} \cdot \frac{\partial\mathbf{W}}{\partial\mathbf{A}} = \nabla_{\mathbf{W}}\mathcal{L} J_A(\mathbf{B})^\top \\
\nabla_{\mathbf{B}}\mathcal{L} &= \frac{\partial\mathcal{L}}{\partial\mathbf{W}} \cdot \frac{\partial\mathbf{W}}{\partial\mathbf{B}} = J_B(\mathbf{A})^\top \nabla_{\mathbf{W}}\mathcal{L}
\end{aligned}$$

Hence, the Fisher Information Matrices can be expressed as:

$$\mathbf{F_A} \approx J_A(\mathbf{B})^\top \mathbf{F_W} J_A(\mathbf{B}), \quad \mathbf{F_B} \approx J_B(\mathbf{A})^\top \mathbf{F_W} J_B(\mathbf{A})$$

The EWC regularization term in the low-rank parameter space is defined as:

$$\mathcal{R}_{\mathbf{A},\mathbf{B}} = \frac{1}{2}\Delta\mathbf{a}^\top \mathbf{F_A} \Delta\mathbf{a} + \frac{1}{2}\Delta\mathbf{b}^\top \mathbf{F_B} \Delta\mathbf{b}$$

The regularization term $\mathcal{R}_{\mathbf{A},\mathbf{B}}$ captures independent penalties in the factor space. Unless the cross-covariance term $\mathbf{F}_{\mathbf{A},\mathbf{B}}$ is explicitly computed and retained, the interaction between $\mathbf{A}$ and $\mathbf{B}$ is ignored. Consequently, the two regularizations cannot be equal, except in special cases such as when only $\mathbf{A}$ or $\mathbf{B}$ is updated. In contrast, estimating $\mathbf{F_W}$ in the full-dimensional space avoids this issue and captures the true sensitivity of the model to perturbations. Therefore, regularization in the full space better preserves the true geometry and parameter importance induced by the low-rank update, providing a more faithful and effective constraint on $\mathbf{A}$ and $\mathbf{B}$.

### A.1.2 Fisher Information Consistency with the Trainable Parameter Space

**Proposition 2.** *Consider a parameterization:*

$$\mathbf{W} = \mathbf{W}_0 + \mathbf{AB}$$

*where $\mathbf{W}_0$ is fixed and only $\mathbf{A}, \mathbf{B}$ are trainable. Let*

$$\theta = \begin{bmatrix} \mathrm{vec}(\mathbf{A}) \\ \mathrm{vec}(\mathbf{B}) \end{bmatrix}, \quad \mathbf{w} = \mathrm{vec}(\mathbf{W}).$$

*Then, the Fisher Information Matrix with respect to $\theta$ satisfies*

$$\mathbf{F}_\theta \;=\; \mathbf{J}^\top \mathbf{F_W} \mathbf{J},$$

*where $\mathbf{F_W}$ is the Fisher Information Matrix with respect to $\mathbf{w}$, and $\mathbf{J} = \partial\mathbf{w}/\partial\theta$ is the Jacobian of the reparameterization.*

***Proof.*** Let $\mathcal{L}(\mathbf{W})$ denote the loss (negative log-likelihood). By the chain rule,

$$\nabla_\theta \mathcal{L} \;=\; \mathbf{J}^\top \nabla_{\mathbf{W}} \mathcal{L}$$

The Fisher Information Matrix with respect to $\theta$ is defined as:

$$\mathbf{F}_\theta = \mathbb{E}\big[\, \nabla_\theta \log p \; \nabla_\theta \log p^\top \,\big]$$

Substituting the chain rule,

$$\begin{aligned} \mathbf{F}_\theta &= \mathbb{E}\big[\, (\mathbf{J}^\top \nabla_{\mathbf{w}} \log p)(\mathbf{J}^\top \nabla_{\mathbf{w}} \log p)^\top \,\big] \\ &= \mathbf{J}^\top \, \mathbb{E}\big[\, \nabla_{\mathbf{w}} \log p \; \nabla_{\mathbf{w}} \log p^\top \,\big] \; \mathbf{J}. \end{aligned}$$

The term inside the expectation is precisely the Fisher Information Matrix with respect to $\mathbf{w}$, denoted $\mathbf{F_W}$. Hence we have:

$$\mathbf{F}_\theta = \mathbf{J}^\top \mathbf{F_W} \mathbf{J} \tag{7}$$

The Jacobian structure has been illustrated in Proposition 1. The Fisher Information Matrix is fundamentally an estimation of the curvature of the loss function with respect to the trainable parameters. Eq. 7 shows that the correct Fisher matrix for $\theta$ is obtained by projecting $\mathbf{F_W}$ into the subspace spanned by $\mathbf{A}$ and $\mathbf{B}$ via $\mathbf{J}$. Computing $\mathbf{F_W}$ directly in the full parameter space $\mathbf{W}$ introduces directions corresponding to the frozen $\mathbf{W}_0$, which are irrelevant for training. Thus, Fisher should be consistently defined in the trainable subspace.

### A.1.3 Constraining Low-Rank Updates via Full-Space Fisher Regularization

**Proposition 3.** *Let the adapted weight matrix be:* $\mathbf{W} = \mathbf{W}_0 + \Delta\mathbf{W} = \mathbf{W}_0 + \mathbf{AB}$*, where* $\mathbf{W}_0$ *denotes the frozen pre-trained weights and* $\Delta\mathbf{W} = \mathbf{AB}$ *is the low-rank update. Then, the empirical Fisher Information Matrix* $\mathbf{F}_{\Delta\mathbf{W}}$ *is estimated by the squared gradients of the log-likelihood with respect to* $\mathbf{W}$*. Consequently, the Fisher regularization on* $\Delta\mathbf{W}$ *induces constraints on the update directions of the low-rank factors* $\mathbf{A}$ *and* $\mathbf{B}$*.*

***Proof.*** Since $\mathbf{W}_0$ is constant and only $\Delta\mathbf{W}$ is trainable, the loss function $\mathcal{L}$ depends on $\mathbf{W}$ only through $\Delta\mathbf{W}$. Therefore, the gradients satisfy $\nabla_{\mathbf{W}}\mathcal{L} = \nabla_{\Delta\mathbf{W}}\mathcal{L}$, because $\partial\Delta\mathbf{W}/\partial\mathbf{W} = \mathbf{I}$. Let $\mathbf{F}_{\mathbf{W}}$ denote the empirical Fisher Information Matrix estimated over weight matrix $\mathbf{W}$:

$$\mathbf{F}_{\mathbf{W}} = \mathbb{E}_{x\sim\mathcal{D}}\left[\mathrm{vec}(\nabla_{\mathbf{W}}\mathcal{L})\,\mathrm{vec}(\nabla_{\mathbf{W}}\mathcal{L})^\top\right]$$

Using the gradient equivalence above, the Fisher matrix in the $\Delta\mathbf{W}$ space is identical:

$$\mathbf{F}_{\Delta\mathbf{W}} = \mathbb{E}_{x\sim\mathcal{D}}\left[\mathrm{vec}(\nabla_{\Delta\mathbf{W}}\mathcal{L})\,\mathrm{vec}(\nabla_{\Delta\mathbf{W}}\mathcal{L})^\top\right] = \mathbf{F}_{\mathbf{W}}$$

For notational simplicity, we omit the $\mathrm{vec}(\cdot)$ operator and treat $\mathbf{W}$ as a vectorized parameter. The Fisher regularization term can be defined as:

$$\mathcal{R}_{\mathbf{W}} = \frac{1}{2}(\mathbf{W} - \mathbf{W}^*)^\top\mathbf{F}_{\mathbf{W}}(\mathbf{W} - \mathbf{W}^*) = \frac{1}{2}\Delta\mathbf{W}^\top\mathbf{F}_{\Delta\mathbf{W}}\Delta\mathbf{W}$$

The gradients of $\mathcal{R}_{\mathbf{W}}$ with respect to $\mathbf{A}$ and $\mathbf{B}$ are:

$$\nabla_{\mathbf{A}}\mathcal{R}_{\mathbf{W}} = \nabla_{\Delta\mathbf{W}}\mathcal{R}_{\mathbf{W}}\cdot\mathbf{B}^\top = \mathbf{F}_{\Delta\mathbf{W}}\Delta\mathbf{W}\cdot\mathbf{B}^\top$$
$$\nabla_{\mathbf{B}}\mathcal{R}_{\mathbf{W}} = \mathbf{A}^\top\cdot\nabla_{\Delta\mathbf{W}}\mathcal{R}_{\mathbf{W}} = \mathbf{A}^\top\cdot\mathbf{F}_{\Delta\mathbf{W}}\Delta\mathbf{W}$$

with:

$$\nabla_{\Delta\mathbf{W}}\mathcal{R}_{\mathbf{W}} = \mathbf{F}_{\Delta\mathbf{W}}\Delta\mathbf{W}$$

Therefore, by propagating the gradient through the low-rank decomposition $\Delta\mathbf{W} = \mathbf{AB}$, the Fisher regularization over $\Delta\mathbf{W}$ imposes a constraint on the update directions of the low-rank factors.

## A.2 Implementation Details

This section provides additional details on the method described in Section 3 and the experimental setup in Section 4 of the main text. In particular, we present the algorithm of EWC-LoRA and discuss the effects of hyperparameters, accompanied by additional ablation studies.

### A.2.1 Optimization Algorithms

Algorithm 1 outlines the learning procedure of EWC-LoRA across tasks $\mathcal{T}_1$ to $\mathcal{T}_T$. At each task, the model is updated via low-rank adaptation while incorporating EWC regularization computed from the Fisher Information Matrix. Unlike prior methods that assign task-specific modules, EWC-LoRA regularizes a shared LoRA, thereby maintaining constant memory cost. For clarity, the key equation referenced in the main text is restated here.

$$\mathcal{L}'_t(\mathbf{A},\mathbf{B}) = \mathcal{L}_t(\mathbf{A},\mathbf{B}) + \frac{\lambda}{2}\,\mathrm{vec}(\mathbf{AB})^\top\mathbf{F}^{\mathrm{cum}}_{t-1}\,\mathrm{vec}(\mathbf{AB}) \tag{3}$$

where $\mathrm{vec}(\mathbf{AB})$ is flattened $\mathbf{AB}$. $\mathbf{F}^{\mathrm{cum}}_t$ denotes the accumulated Fisher matrix obtained from task $\mathcal{T}_{t-1}$. $\lambda$ is the regularization strength.

**Algorithm 1:** The learning procedure of EWC-LoRA.

**Input:** A sequence of tasks $\{\mathcal{T}_t\}_{t=1}^{T}$ with datasets $\{\mathcal{D}_t\}_{t=1}^{T}$; A frozen pre-trained model with parameters $\mathbf{W}_0 \in \mathbb{R}^{d_O \times d_I}$; Low-rank adaptation matrices $\mathbf{A} \in \mathbb{R}^{d_O \times r}$ and $\mathbf{B} \in \mathbb{R}^{r \times d_I}$, with rank $r$; Task decay factor $\gamma_t = 0.9,\ \forall t = 1, \ldots, T$.

**Output:** Adapted model parameters $\mathbf{W}_T \in \mathbb{R}^{d_O \times d_I}$ that generalize across all tasks $\{\mathcal{T}_t\}_{t=1}^{T}$.

Initialize accumulated Fisher Information Matrix: $\mathbf{F}_0^{\text{cum}} \leftarrow \gamma_{\text{prior}} \cdot \mathbf{I}$ ; `// 0 if no prior`

**for** $t = 1$ **to** $T$ **do**

**Step 1:** Initialize $\mathbf{A} \leftarrow \mathbf{0}$, $\mathbf{B} \leftarrow \mathcal{U}(a, b)$

**Step 2:** Low-rank adaptation on current task $\mathcal{T}_t$: $\mathbf{A}^*, \mathbf{B}^* \leftarrow$ Eq. 3 ;

**Step 3:** Fisher estimation for $\mathcal{T}_t$;

1. Get gradient $\nabla_{\mathbf{W}} \mathcal{L}$ on the full-dimensional space ;
2. Compute diagonal entries of Fisher matrix: $F_t^{i,i} \approx \frac{1}{|\mathcal{D}_t|} \sum_{(x,y) \in \mathcal{D}_t} \left( \frac{\partial \log p_{\mathbf{W}_t^*}(y|x)}{\partial w_i} \right)^2$;
3. Update accumulated Fisher Information Matrix: $\mathbf{F}_t^{\text{cum}} \leftarrow \gamma_t \cdot \mathbf{F}_{t-1}^{\text{cum}} + \mathbf{F}_t$;

**Step 4:** Integrate low-rank parameter: $\mathbf{W}_t = \mathbf{W}_{t-1} + \mathbf{A}^* \mathbf{B}^*$;

**Step 5:** Discard task-specific dataset $\mathcal{D}_t$ and Fisher matrix $\mathbf{F}_t$.

### A.2.2 HYPERPARAMETERS

We follow the training configurations specified by the authors in the original papers. When such configurations are not available, we adopt a unified set of hyperparameters that has been validated to perform reliably across methods, thereby ensuring consistency in our experimental setup. In all experiments, we use the Adam optimizer with $\beta_1 = 0.9$ and $\beta_2 = 0.99$. The number of training epochs depends on the specific dataset, and the training batch size is set to 128. No shuffling is applied during training; however, we verified that enabling shuffling generally leads to improved results. Table 7 summarizes the hyperparameters used during training, with method-specific parameters highlighted for each respective approach.

Table 7: Hyperparameters for different benchmarks and methods. "**lr**" denotes learning rate. For the parameter $\epsilon$, we refer readers to Liang & Li (2024) for details.

| Datasets | Methods |
|---|---|
| CIFAR-100 | **optimizer:** Adam; **schedular:** Cosine; **batch size:** 128; **shuffle:** False; **epochs:** 20; **rank:** 10<br>**lr:** 0.0005; **classifier lr:** 0.005; **lr decay:** 0.1<br>**lr:** 0.008; **classifier lr:** 0.008; **lr decay:** 0.1 (SD-LoRA)<br>$\epsilon$ **:** 0.95 (InfLoRA) |
| DomainNet | **optimizer:** Adam; **schedular:** Cosine; **batch size:** 128; **shuffle:** False; **epochs:** 5; **rank:** 30<br>**lr:** 0.0005; **classifier lr:** 0.005; **lr decay:** 0.1<br>**lr:** 0.02; **classifier lr:** 0.02; **lr decay:** 0.0 (SD-LoRA)<br>$\epsilon$ **:** 0.95 (InfLoRA) |
| ImageNet-R | **optimizer:** Adam; **schedular:** Cosine; **batch size:** 128; **shuffle:** False; **epochs:** 50; **rank:** 10<br>**lr:** 0.0005; **classifier lr:** 0.0005; **lr decay:** 0.1<br>**lr:** 0.01; **classifier lr:** 0.01; **lr decay:** 0.0; **weight decay:** 0.0005 (SD-LoRA)<br>**weight decay:** 0.005 (EWC-LoRA)<br>$\epsilon$ **:** 0.98 (InfLoRA) |
| ImageNet-A | **optimizer:** Adam; **schedular:** Cosine; **batch size:** 128; **shuffle:** False; **epochs:** 10; **rank:** 10<br>**lr:** 0.0005; **classifier lr:** 0.005; **lr decay:** 0.1<br>$\epsilon$ **:** 0.98 (InfLoRA) |

For the regularization strength $\lambda$ in Eq. 3, we evaluated a wide range from $10^1$ to $10^{10}$. The trend is illustrated in Figure 3b of the main text. We observe that across all datasets, when using the empirical Fisher, the best overall performance is achieved around $10^7$. Moreover, with relatively

smaller values of $\lambda$ (e.g., $10^1$ to $10^4$), performance tends to decrease initially. For all experiments, the regularization strength $\lambda$ is set to $10^7$.

For the parameter $\gamma$ in Algorithm 1, we set all tasks to be equally important to $\gamma = 0.9$. To further assess its effect, we evaluated the impact of $\gamma$ on performance using CIFAR-100. We use a single seed for performance comparison. The results are presented in Table 8 and Figure 4. In the figure, each row shows the performance on all previously encountered tasks (x-axis) after learning the current task (y-axis).

Table 8: Performance comparison under different values of $\gamma$ on CIFAR-100.

| | $\gamma = 0.9$ | $\gamma = 0.5$ | $\gamma = 0$ |
|---|---|---|---|
| $\overline{A}_{10}$ | 87.47 | **88.14** | 86.63 |
| Avg. | 92.12 | **92.34** | 92.04 |
| Stability | **94.45** | 94.37 | 91.81 |
| Plasticity | 97.99 | 98.33 | **99.07** |

The parameter $\gamma$ controls the accumulation of Fisher information across tasks in continual learning. When $\gamma = 0$, no Fisher information is carried over from previous tasks, meaning that only the Fisher matrix of the current task is used to regularize the subsequent task. As $\gamma$ increases, past information is accumulated more strongly, which can help preserve knowledge from earlier tasks. We evaluated three settings: $\gamma = 0, 0.5$, and $0.9$. As shown in Table 8, the final accuracy remains relatively similar across these settings; however, the main differences are observed in stability and plasticity. Figure 4 further illustrates that setting $\gamma$ to zero leads to a notable drop in stability, with earlier tasks suffering more severe forgetting, whereas higher $\gamma$ values help maintain performance on previous tasks while still allowing effective learning of new tasks.

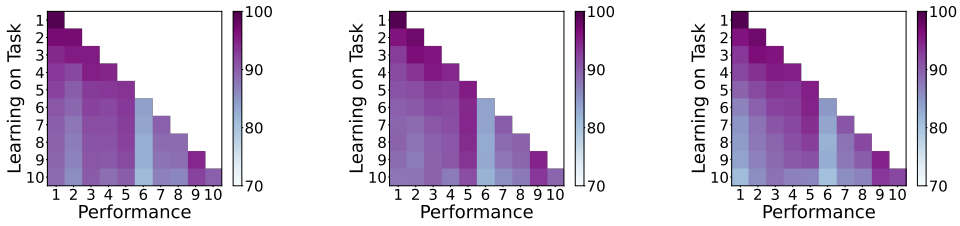


(a) $\gamma = 0.9$ (b) $\gamma = 0.5$ (c) $\gamma = 0$

Figure 4: Task-wise performance on CIFAR-100 under different $\gamma$ settings.

### A.3 Additional Experiments

**Results Across Varied Task Length.** Table 9 reports the full results of low-rank continual learning methods under varying task lengths on ImageNet-R. For EWC-LoRA, the performance gains appear relatively modest, likely due to the inherent domain shift in this benchmark, which may constrain the effectiveness of regularization-based methods for continual adaptation. We further observe that InfLoRA achieves better results on shorter sequences, whereas SD-LoRA performs more strongly on longer sequences. Examining the accuracy matrix for longer sequences, we find that although SD-LoRA exhibits lower stability, its higher plasticity often leads to superior final performance. This observation suggests that model evaluation should go beyond reporting only the final accuracy. It is also important to track performance throughout the task sequence and explicitly report both stability and plasticity.

**Task-wise Performance.** Figure 5 and Figure 6 show the accuracy matrix of the LoRA-based methods on CIFAR-100 and DomainNet. Each row corresponds to the performance on all previously encountered tasks after training on the current task. The diagonal entries correspond to the most recently trained tasks. As expected, Finetune exhibits severe forgetting on previous tasks while maintaining high performance on the current task, as shown in the matrix entries. On CIFAR-100,

Table 9: Comparison results on ImageNet-R across different task lengths (in %).

| Tasks | **ImageNet-R** (N=5) | | **ImageNet-R** (N=20) | |
|---|---|---|---|---|
| Methods | $\overline{A}_5$ (↑) | Avg. (↑) | $\overline{A}_{20}$ (↑) | Avg. (↑) |
| Joint Train | $81.69_{(0.30)}$ | $85.57_{(0.13)}$ | $81.66_{(0.22)}$ | $86.41_{(0.10)}$ |
| Finetune | $69.26_{(0.74)}$ | $78.88_{(0.31)}$ | $47.06_{(2.05)}$ | $63.01_{(0.56)}$ |
| InfLoRA | $\mathbf{77.37}_{(0.30)}$ | $\mathbf{82.19}_{(0.24)}$ | $69.63_{(0.62)}$ | $76.95_{(0.54)}$ |
| SD-LoRA | $74.90_{(1.58)}$ | $79.93_{(0.29)}$ | $\mathbf{72.26}_{(0.37)}$ | $\mathbf{77.81}_{(0.21)}$ |
| Vanilla LoRA | $70.15_{(1.00)}$ | $79.16_{(0.37)}$ | $56.17_{(1.50)}$ | $69.51_{(0.37)}$ |
| EWC-LoRA | $\underline{76.36}_{(0.21)}$ | $\underline{81.43}_{(0.13)}$ | $\underline{70.18}_{(1.06)}$ | $\underline{77.06}_{(0.54)}$ |

we observe that InfLoRA better preserves performance on the earliest task (first column). On DomainNet, SD-LoRA adapts more effectively to new tasks. On both datasets, EWC-LoRA achieves a more balanced trade-off between stability and plasticity compared to the other two methods.

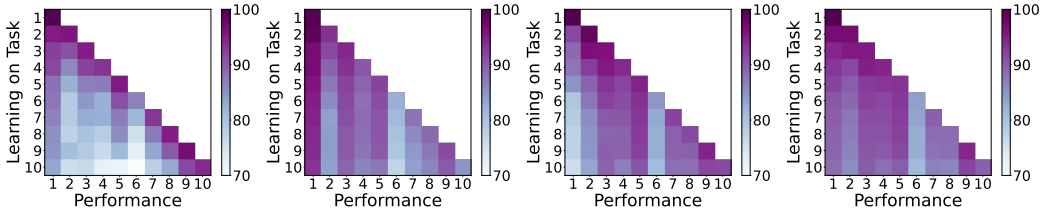


(a) Finetune (b) InfLoRA (c) SD-LoRA (d) EWC-LoRA

Figure 5: Task-wise performance of LoRA-based methods on CIFAR-100. Each row represents the performance on all previously encountered tasks (x-axis) after learning the current task (y-axis).

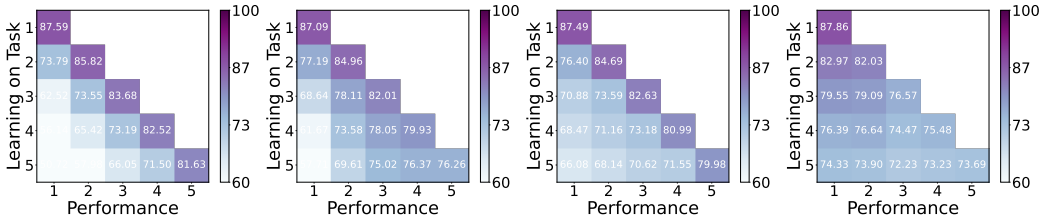


(a) Finetune (b) InfLoRA (c) SD-LoRA (d) EWC-LoRA

Figure 6: Task-wise performance of LoRA-based methods on DomainNet. Each row represents the performance on all previously encountered tasks (x-axis) after learning the current task (y-axis).

**Precomputed Fisher.** As illustrated in Xiang et al. (2023) and Šliogeris et al. (2025), they use a precomputed Fisher Information Matrix to preserve prior knowledge. Following this approach, we evaluate performance when a Fisher Information Matrix is precomputed and used throughout the continual learning process. Unlike these works, we do not rely on a large-scale dataset to compute the Fisher matrix. We consider two settings: (1) Uniform parameter importance: All parameters are assigned equal importance, i.e., $\gamma_{\text{prior}}$ in Algorithm 1 is set to a constant, and the Fisher matrix is an identity matrix. (2) Dataset-based Fisher: The Fisher Information Matrix is computed in advance using the entire dataset. The results are shown in Table 10. We observe that the uniform Fisher exhibits lower stability, while the plasticity of both methods is similar, but still much lower than ours. This suggests that using a precomputed, fixed Fisher imposes stronger constraints on the weights, thereby limiting plasticity. As expected, the dataset-based Fisher achieves higher stability than the uniform Fisher, which is reasonable since it better captures the true importance of the parameters.

Table 10: Regularization using precomputed Fisher on CIFAR-100.

| **Strategy** | $\overline{A}_{10}$ | Avg. | Stability | Plasticity |
|---|---|---|---|---|
| Uniform $\mathbf{F} = \mathbf{I}$ | 83.02 | 88.85 | 92.26 | 94.63 |
| Dataset-based $\mathbf{F}$ | 83.87 | 89.36 | 93.15 | 94.74 |

**Trade-off between Stability and Plasticity.** To better understand how different methods balance stability and plasticity, we introduce a trade-off metric that approximates this balance:

$$\mathrm{T} = \frac{2 \cdot S \cdot P}{S + P} \tag{8}$$

where $S$ and $P$ denote the Stability and Plasticity, respectively, as defined in Eq. 5 and Eq. 6. Figure 7 illustrates the trade-off between stability and plasticity for different low-rank CL methods. Vanilla LoRA generally achieves the highest plasticity, as it does not include mechanisms to prevent forgetting. EWC-LoRA attains stability comparable to InfLoRA, while retaining more plasticity than InfLoRA. Overall, EWC-LoRA achieves the best trade-off among the methods.

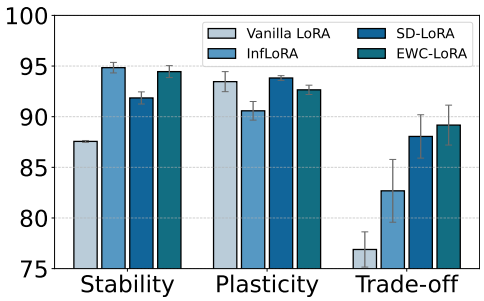


Figure 7: Trade-off between stability and plasticity.

**Computation on Fisher Information Matrix.** As suggested by van de Ven (2025), we investigate different methods for estimating the FIM. The results are presented in Table 11. Here, "Exact" indicates that the inner expectation in Eq. 4 is computed exactly for each training sample. "Exact (n=500)" denotes that the outer expectation is calculated using a subset of 500 samples from the old training data. "Sample" indicates that the inner expectation is computed over a sampled class. The results indicate that the optimal regularization strength varies according to the estimation method. In general, the Exact Fisher outperforms the Empirical Fisher, requiring a smaller regularization strength. The Sample method yields slightly better results than the Empirical Fisher.

Table 11: Different ways for estimating the Fisher matrix. Final accuracy of each variant using its optimal strength $\lambda$ on CIFAR-100.

| Estimation | $\overline{A}_{10}$ | Avg. | Best $\lambda$ |
|---|---|---|---|
| Exact | 88.32 | 92.77 | $\lambda = 10^5$ |
| Exact (n=500) | 88.28 | 92.76 | $\lambda = 10^5$ |
| Sample | 88.10 | 92.50 | $\lambda = 10^7$ |
| Empirical | 87.91 | 92.27 | $\lambda = 10^7$ |

### A.4 The Use of Large Language Models (LLMs)

In the preparation of this manuscript, the LLM was used to refine sentence structures, ensure clarity, and improve the readability of the text.